Supporting Information

Underlying factors of mega pressure hysteresis in cerium-rich $CaCu_5$-type metal hydrides and effective modification strategies

Panpan Zhou [a,1], Jianwei Zhang [b,1], Jiapeng Bi [a,1], Xuezhang Xiao [a,c,*], Ziming Cao [a], Liujun Zhan [a], Huahai Shen [d], Miao Lu [e], Zhinian Li [e], Yuyuan Zhao [f], Li Wang [f], Mi Yan [a,f,*], and Lixin Chen [a,*]

[a] *State Key Laboratory of Silicon and Advanced Semiconductor Materials; School of Materials Science and Engineering, Zhejiang University, Hangzhou 310027, China.*

[b] *School of Physics, University of Electronic Science and Technology of China, Chengdu 610054, China*

[c] *Key Laboratory of Advanced Materials and Applications for Batteries of Zhejiang Province, Hangzhou 310013, Zhejiang, China.*

[d] *Institute of Nuclear Physics and Chemistry, China Academy of Engineering Physics, Mianyang 621900, China.*

[e] *Institute of Energy Materials and Technology, General Research Institute for Non-ferrous Metals, Beijing 100088, China.*

[f] *Baotou Research Institute of Rare Earths, Baotou 014030, China.*

[*] Corresponding author.

Email: lxchen@zju.edu.cn (L.X. Chen), xzxiao@zju.edu.cn (X.Z. Xiao), mse_yanmi@zju.edu.cn (M. Yan)

[1] These authors contributed equally.

Supplemental Tables

Table S1. The thermodynamic properties of La-Ce-Ni based alloys during de-/hydrogenation process.

$La_{1-x}Ce_xNi_5$	$x = 0$	$x = 0.2$	$x = 0.4$	$x = 0.6$	$x = 0.8$	$x = 1.0$
ΔH_a (kJ.mol^{-1})	-28.23±0.33	-24.77±0.05	-25.46±0.54	-20.61±0.66	-17.64±0.47	-15.73*±0.07*
ΔS_a (J.mol^{-1}. K^{-1})	-102.39±1.08	-99.00±0.17	-109.49±1.78	-100.93±2.20	-98.74±1.54	-100.58*±0.24*
$\Delta G_{a,\ 293.15K}$ (kJ.mol^{-1})	1.78	4.25	6.63	8.96	11.31	13.72*
ΔH_d (kJ.mol^{-1})	30.33±0.23	27.78±0.86	27.18±1.02	21.78±0.11	21.03±1.39	18.30*±1.09*
ΔS_d (J.mol^{-1}. K^{-1})	106.14±0.75	103.15±2.83	106.07±3.37	93.65±0.38	96.50±4.58	92.76*±3.59*
$\Delta G_{d,\ 293.15K}$ (kJ.mol^{-1})	-0.79	-2.48	-3.94	-5.68	-7.28	-8.88*

Table S2. The average mechanical properties of bulk $LaNi_5$ polycrystal.

Mechanical Properties	Voigt	Reuss	Hill
Bulk Modulus B / GPa	136.46	135.640	136.049
Young's Modulus E / GPa	160.68	157.015	159.015
Shear Modulus G / GPa	61.62	60.211	60.916
Poisson's Ratio v	0.30	0.307	0.305
P-wave Modulus / GPa	218.62	215.921	217.270
Pugh's Ratio B/G	2.21	2.253	2.233
Vickers Hardness-1 / GPa	5.75	5.459	5.603
Vickers Hardness-2 / GPa	6.89	6.649	6.770

Table S3. The average mechanical properties of bulk $CeNi_5$ polycrystal.

Mechanical Properties	Voigt	Reuss	Hill
Bulk Modulus B / GPa	152.08	151.532	151.805
Young's Modulus E / GPa	174.82	170.808	172.819
Shear Modulus G / GPa	66.81	65.088	65.948
Poisson's Ratio v	0.31	0.312	0.310
P-wave Modulus / GPa	241.16	238.316	239.736
Pugh's Ratio B/G	2.28	2.328	2.302
Vickers Hardness-1 / GPa	5.88	5.519	5.698
Vickers Hardness-2 / GPa	7.07	6.768	6.920

Table S4. The crystallographic data of $RENi_5$-based alloys.

Atomic number	Alloy	Atomic radius / pm	Electron Configuration	Lattice parameters / Å		a/c	Unit cell volume /Å^3
				a	c		
57	$LaNi_5$	187	6s2 5d1	5.0170	3.9810	1.2602	86.78
58	$CeNi_5$	181	6s2 4f1 5d1	4.8750	4.0100	1.2157	82.53
59	$PrNi_5$	182	6s2 4f3	4.9470	3.9830	1.2420	84.42
60	$NdNi_5$	182	6s2 4f4	4.9478	3.9750	1.2447	84.27
61	$PmNi_5$	183	6s2 4f5	-	-	-	-
62	$SmNi_5$	181	6s2 4f6	4.9300	3.9700	1.2418	83.56
63	$EuNi_5$	199	6s2 4f7	4.9225	3.9631	1.2421	83.16
64	$GdNi_5$	179	6s2 4f7 5d1	4.9020	3.9640	1.2366	82.49
65	$TbNi_5$	180	6s2 4f9	4.8940	3.9660	1.2340	82.26
66	$DyNi_5$	180	6s2 4f10	4.8760	3.9670	1.2291	81.67
67	$HoNi_5$	179	6s2 4f11	4.8732	3.9625	1.2298	81.49
68	$ErNi_5$	178	6s2 4f12	4.8540	3.9640	1.2245	80.88
69	$TmNi_5$	177	6s2 4f13	4.8340	3.9700	1.2176	80.34
70	$YbNi_5$	176	6s2 4f14	4.8260	3.9760	1.2138	80.20
71	$LuNi_5$	175	6s2 4f14 5d1	4.8340	3.9690	1.2179	80.32

Supplemental Figures

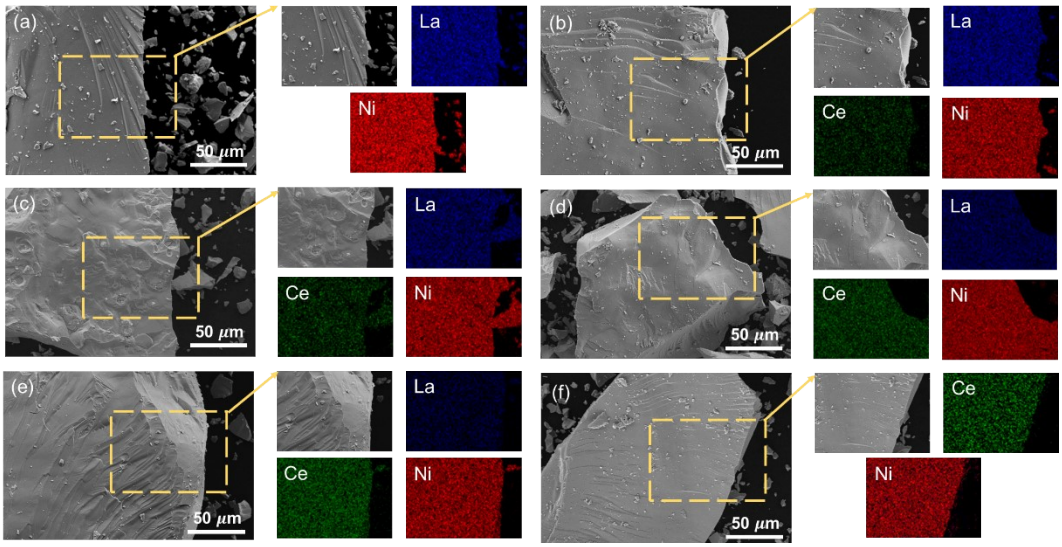

Figure S1. SEM images with related EDS mappings of (a) $LaNi_5$, (b) $La_{0.8}Ce_{0.2}Ni_5$, (c) $La_{0.6}Ce_{0.4}Ni_5$, (d) $La_{0.4}Ce_{0.6}Ni_5$, (e) $La_{0.2}Ce_{0.8}Ni_5$, (f) $CeNi_5$.

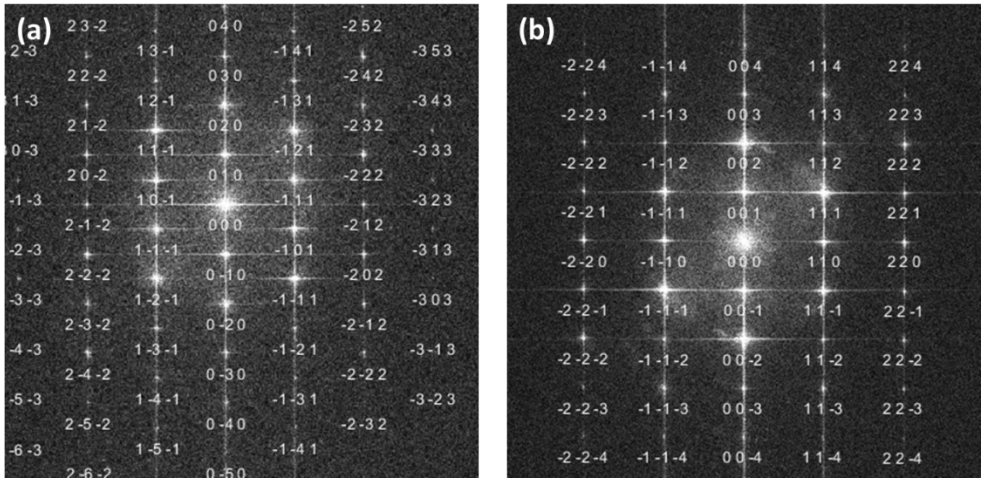

Figure S2. Calibration detail information for specific plane after fast Fourier transform (FFT) treatment for Figure 1 (d-g) and Figure 1 (h-k) of $LaNi_5$ and $CeNi_5$ TEM cross-sectional samples: (a) z-axis along the direction of [101], (b) z-axis along the direction of [1-10].

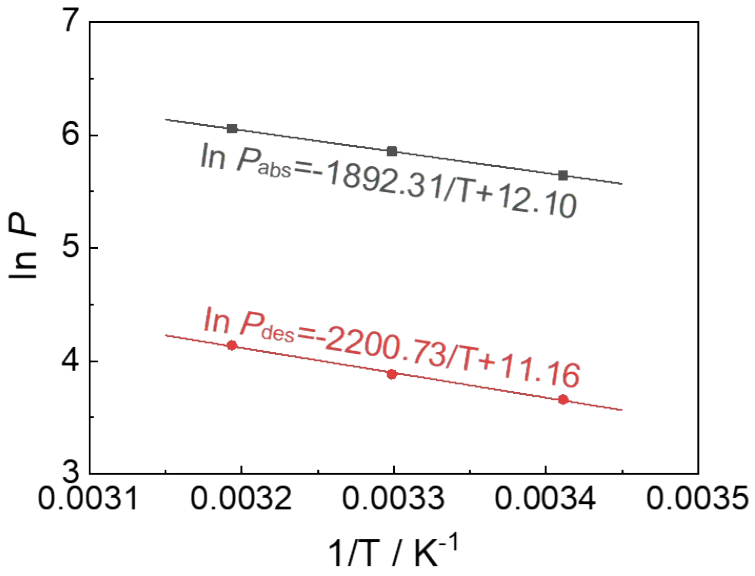

Figure S3. De-/Hydrogenation Van't Hoff curves of $CeNi_5$ alloy based on the derived equilibrium pressure values.

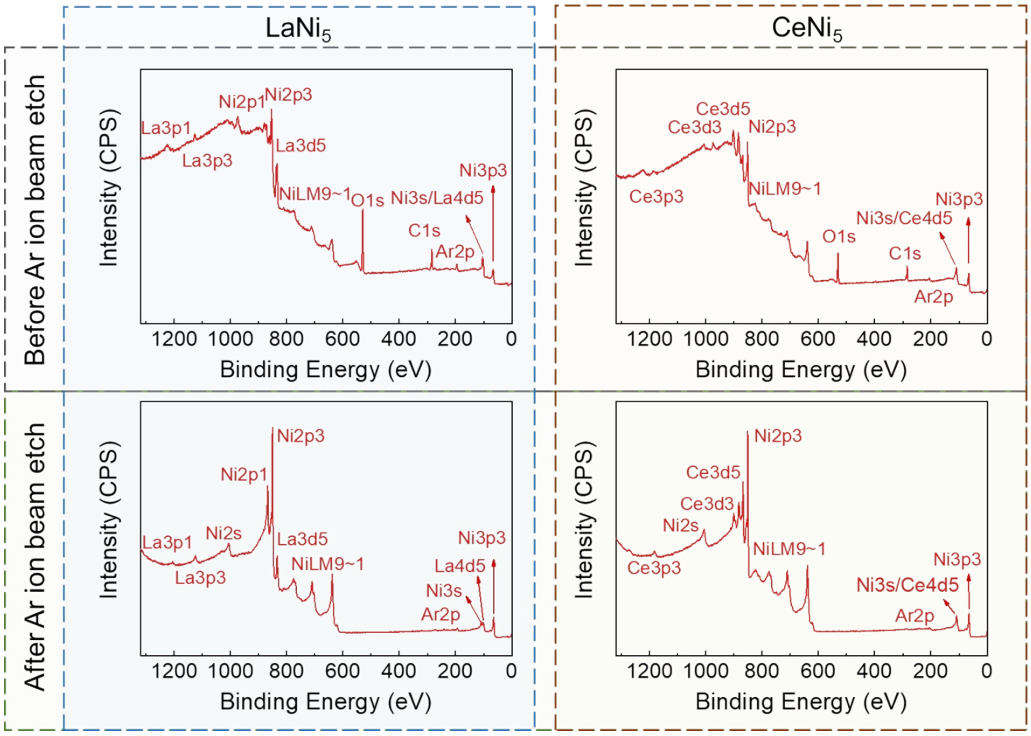

Figure S4. XPS survey of $LaNi_5$ and $CeNi_5$ before and after Ar ion beam etch.

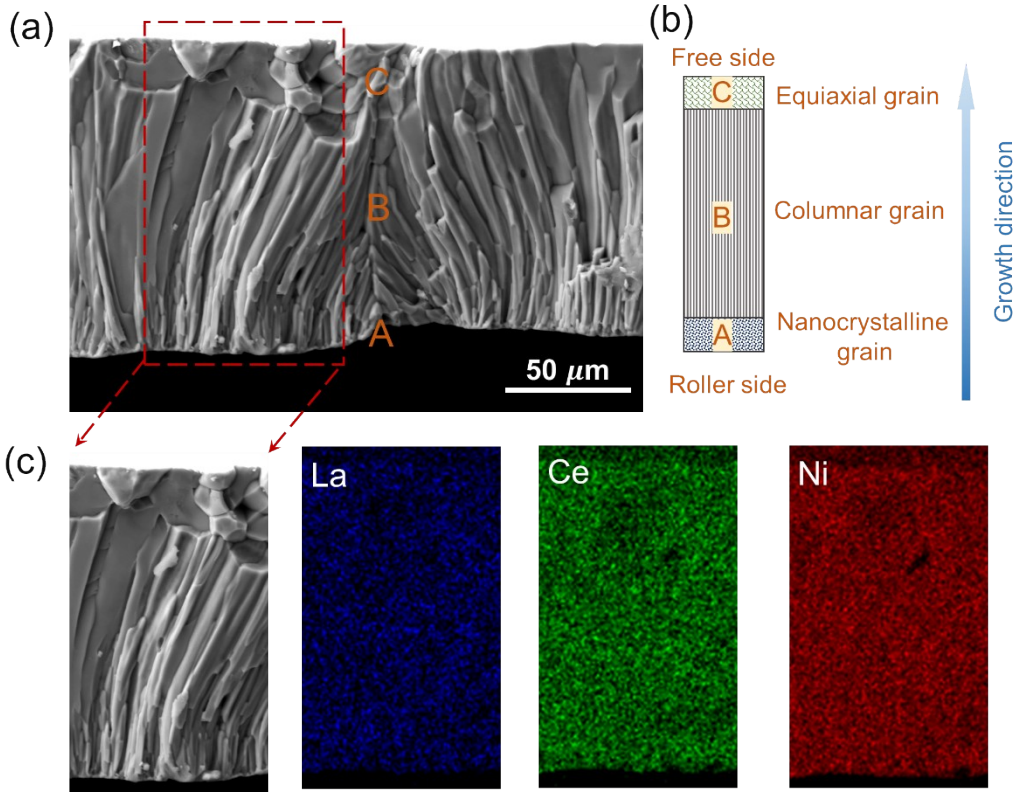

Figure S5. (a) SEM images of $La_{0.2}Ce_{0.8}Ni_5$ alloy prepared through melt spun-40 m/s; (b) Illustration of related cross-section grain structure; (c) EDS mappings of elemental composition.

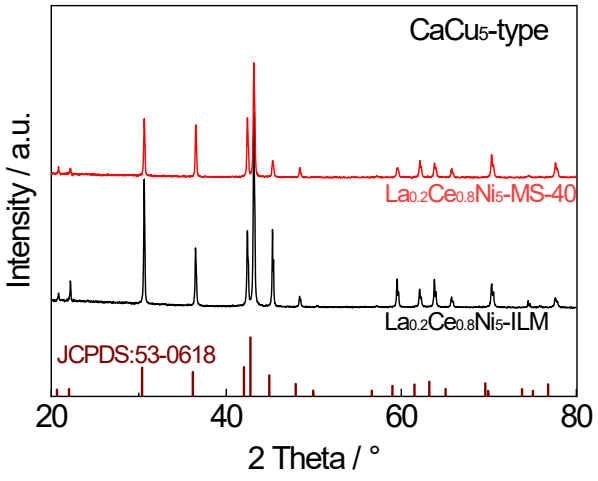

Figure S6. XRD patterns of $La_{0.2}Ce_{0.8}Ni_5$ alloy that prepared through ILM and MS-40.

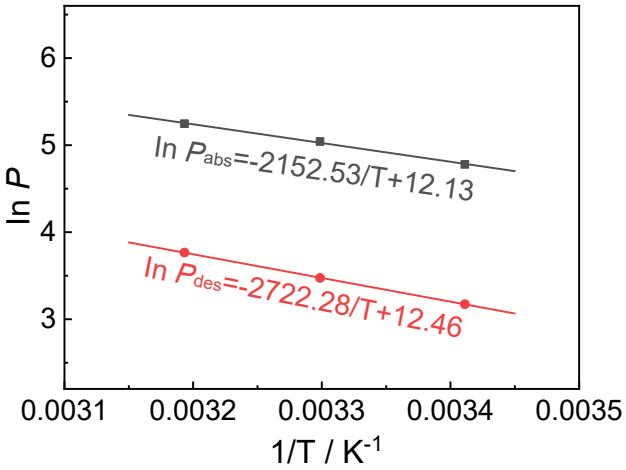

Figure S7. De-/Hydrogenation Van't Hoff curves of $La_{0.2}Ce_{0.8}Ni_5$ alloy prepared through MS-40.